Bull. Chem. Soc. Jpn., 72, 639—651 (1999)

Magnetic Properties of TTF-Type Charge Transfer Salts in the Mott Insulator Regime

Naoki Yoneyama,* Akira Miyazaki, Toshiaki Enoki,* and Gunzi Saito†

Department of Chemistry, Tokyo Institute of Technology, Ookayama, Meguro-ku, Tokyo 152-8551

†Department of Chemistry, Kyoto University, Sakyo-ku, Kyoto 606-8244

(Received September 11, 1998)

We have investigated the magnetic properties of several TTF-based Mott insulators consisting of dimerized/trimerized-donor units, which are classified into three subgroups: (1) β'-(BEDT-TTF)$_2$X (X = ICl_2, $AuCl_2$) and (BEDT-TTF)$_2GaCl_4$ as strong dimer systems, (2) α'-(BEDT-TTF)$_2IBr_2$ salt as a weak dimer system, and (3) (BMDT-TTF)$_3ClO_4$(1,2-dichloroethane) and (BMDT-TTF)$_3AsF_6$(1,1,2-trichloroethane) as weak trimer systems. The group (1) compounds have localized spin systems with an $S = 1/2$ localized spin per dimer unit. In group (2), weak dimerization produces a fractional magnetic moment, which reflects the delocalization of the electrons, although the magnetism is described in terms of an $S = 1/2$ low-dimensional antiferromagnet. The ClO_4 salt in the group (3) indicates the existence of a localized spin per trimer, whereas the trimerization is quite weak, because the inter-trimer Coulomb interactions generate the charge disproportionation resulting in the localization of electrons. The absence of the charge disproportionation brings about the feature of fractional magnetic moments in the AsF_6 salts.

A large number of TTF-based organic charge transfer salts have been synthesized with various kinds of anions. The result is a large variety of low dimensional systems consisting of π-electrons, from metallic states to insulating states. The variety of electronic states is caused by the competition between the transfer integral and the Coulomb interaction; that is, a metallic state appears when the transfer integral is superior to the Coulomb interaction, whereas the Coulomb interaction being superior to the transfer integral leads to an insulating state as a Mott insulator, where the π-electrons are localized on the donor molecules. The insulating state, where the one-electron band picture on the electronic state fails, results in the appearance of localized magnetic moments on the molecules, which is the most characteristic feature of these compounds as localized spin systems. Consequently, the localized magnetic moments of the π-electrons aligned on the low-dimensional lattice of the molecules provide a low-dimensional magnetic system. Actually the resistivities of these materials are semiconductive while the susceptibilities are relatively larger than those of metallic materials or of band insulating materials.[1] The correlation between the resistivities and the susceptibilities at room temperature is mapped in Fig. 1 for various charge transfer salts[1—14] to see how Mott insulators are positioned. Here, we classify the charge transfer salts into Mott insulators, metals, and band insulators based on the temperature dependence of the resistivity and the behavior of the susceptibilities. Namely, the insulators are defined as the materials whose conductivity is explained in terms of an activation process, while the conductivity shows an increasing trend with lowering of the temperature in the metals. The Mott insulator is characterized by the presence of localized magnetic moments whose values are expected for $S = 1/2$, whereas no localized spins are present in the band insulator. As explained consistently with the definitions, the Mott insulators occupy a specific region (shaded area) having large resistivities and susceptibilities, most of which are isolated from the metallic compounds (circles) and the band insulators (diamond). It is worth noting that the application of pressure, which works to reduce the resistivities, makes Mott insulators change to metals through a critical region.

Here, we have a group of molecular-based Mott insulators which have a specific structural feature; that is, dimerization/trimerization of donor molecules in their crystals. In these materials, the strength of the on-site Coulomb interaction is roughly represented by that of the intra-dimer/trimer transfer integral (t_{intra}),[15] which is in the same order of magnitude to the inter-dimer/trimer transfer integral (t_{inter}). Therefore, the ratio between t_{intra} and t_{inter}, which depends on the degree of dimerization/trimerization, and therefore, can be controlled by changing temperature and/or pressure, is varied to make a systematic investigation with a large variety of Mott insulators including those located just around the metal–insulator border.

The purpose of this paper, therefore, is to investigate systematically the magnetic properties of dimer/trimer-based Mott insulators by means of the magnetic susceptibilities and ESR spectra. We overview the crystal structures of the salts targeted in the present work, from the view of the dimer/trimer-unit structure, which are located at representative points in the Mott insulator region (shaded area) in Fig. 1. First, we pick up β'-(BEDT-TTF)$_2$X (X = ICl_2,[16,17]

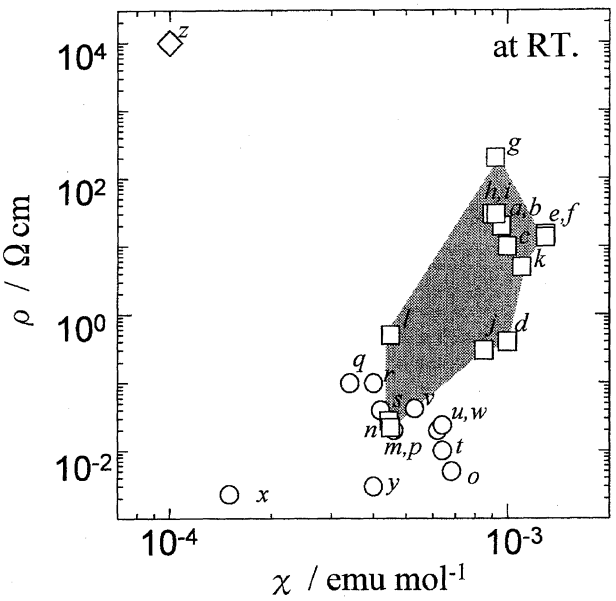

Fig. 1. The diagram of the resistivities vs. susceptibilities at room temperature for various TTF-based charge transfer salts; Mott insulators (square; β'-(BEDT-TTF)$_2$X (X = ICl_2 (*a*), $AuCl_2$ (*b*)), (BEDT-TTF)$_2GaCl_4$ (*c*), α'-(BEDT-TTF)$_2IBr_2$ (*d*), (BMDT-TTF)$_3ClO_4$(1,2-dichloroethane) (*e*), (BMDT-TTF)$_3AsF_6$(1,1,2-trichloroethane) (*f*), α'-(BEDT-TTF)$_2$X (X = $AuBr_2$ (*g*),[2] $CuCl_2$ (*h*),[2] $Ag(CN)_2$ (*i*),[2] $Au(CN)_2$ (*j*),[3] (C_1TET-TTF)$_2$Br (*k*),[4] $\varkappa$-(BEDT-TTF)$_2$Cu[N(CN)$_2$]Cl (*l*),[5] $\varkappa$-(BEDT-TTF)$_2$Cu[N(CN)$_2$]Br (*m*),[6] and $\varkappa$-(BEDT-TTF)$_2$Cu(SCN)$_2$ (*n*).[7]), metallic compounds (circle; α-(BEDT-TTF)$_2I_3$ (*o*),[8] β-(BEDT-TTF)$_2$X (X = I_3 (*p*),[8] AuI_2 (*q*),[9]) TTF_2CuCl_2 (*r*),[10] (BEDT-TTF)$_2ClO_4$(1,1,2-trichloroethane)$_{0.5}$ (*s*),[1] (BEDT-TTF)$_2BF_4X_{0.5}$ (X = 1,1,2-trichloroethane (*t*), 1,2-dibromoethane (*u*), 1,2-dichloroethane (*v*)),[11] (BEDT-TTF)$_3(ClO_4)_2$ (*w*),[1] (TMTSF)$_2AsF_6$ (*x*),[12] and (BMDT-TTF)$_2$Au(CN)$_2$ (*y*)[13]), band insulators (diamond; (BEDT-TTF)HgBr$_3$ (*z*)[14]).

$AuCl_2$[18,19]) which hereafter will be referred to as the β'-ICl_2 salt and the β'-$AuCl_2$ salt, respectively, or the β'-salts, where BEDT-TTF is bis(ethylenedithio)tetrathiafulvalene. These two salts with marks *a* and *b* are located around the top of the region, which have the same structure as schematically shown in Fig. 2(a), where BEDT-TTF molecules are strongly dimerized with face-to-face contacts. Second, we deal with (BEDT-TTF)$_2GaCl_4$,[20] referred to as the $GaCl_4$ salt. The crystal structure shown in Fig. 2(b) consists of four crystallographically independent BEDT-TTF molecules (molecules A, B, C, and D), which are stacked along the *b*-axis in the formation of dimerized A–B and C–D pairs. The $GaCl_4$ salt marked by *c* is located near the β'-salts in the region. Thus, these three salts are expected to have the similar characteristic features. Third, we deal with α'-(BEDT-TTF)$_2IBr_2$[21,22] (referred to as the α'-IBr_2 salt) which is located at the lower right place (*d*) in the region. The structure of this compound shown in Fig. 2(c) contains two independent BEDT-TTF molecules (molecules A and B) coupled weakly through the largest transfer integral (t_{b2}), which are arranged on the *ab*-plane. It is worth noting that the strongest transfer integral does not necessarily feature face-to-face inter-molecular contacts as shown in Fig. 2(c). Finally, we discuss two isostructural weak trimer systems (BMDT-TTF)$_3ClO_4$(1,2-dichloroethane)[23,24] and (BMDT-TTF)$_3AsF_6$(1,1,2-trichloroethane),[25] referred to as the ClO_4 salt and the AsF_6 salt, respectively, or the 3 : 1 salts, where BMDT-TTF is bis(methylenedithio)tetrathiafulvalene. The crystal structure of these salts, schematically shown in Fig. 2(d), has two independent BMDT-TTF molecules, A and B. The donor molecules are stacked in the face-to-face manner along the *a*-axis, although the largest transfer integral t_{c3} along the diagonal side-by-side direction gives leaning trimer units. These 3 : 1 salts are located at the right-side edge of the Mott insulator region.

We consider that these six typical salts cover the whole Mott-type insulator region except the bottom and left-side parts of the region where well investigated $\varkappa$-type salts (marked by *l*, *m*, and *n*)[5–7] are located.

Experimental

All the single crystals were prepared electrochemically as described in the references for the β'-ICl_2 salt,[17] the β'-$AuCl_2$ salt,[18,19] the $GaCl_4$ salt,[20] the α'-IBr_2 salt,[26] and the ClO_4 salt.[23] The AsF_6 salt was synthesized by means of electrocrystallization using BMDT-TTF (3 mg), 1,1,2-trichloroethane (15 ml), and supporting electrolyte (n-$C_4H_9)_4NAsF_6$ (40 mg) with a constant current of about 0.5 μA in the period of one week. The typical sample size was ca. $1.2\times0.4\times0.1$ mm^3 (corresponding to the *c*-, b^*-, and a^*-axes, respectively) for the β'-ICl_2 salt, ca. $0.8\times0.2\times0.1$ mm^3 for the β'-$AuCl_2$ salt (*c*-, b^*-, and a^*-axes), ca. $0.8\times0.1\times0.05$ mm^3 (*c*-, b^*-, and a^*-axes) for the $GaCl_4$ salt, ca. $1\times0.8\times0.01$ mm^3 (*a*-, *b*-, and c^*-axes) for the α'-IBr_2 salt, ca. 1×1 mm^2 (*a*- and *c*-axes, very thin plate) for the ClO_4 and AsF_6 salts. The cell constants were checked by X-ray diffraction for all the compounds.

The crystal structure of the AsF_6 salt was analyzed using a Rigaku AFC-7 automated diffractometer with Mo $K\alpha$ radiation. The analysis carried out by the direct method gave a final *R*-value of 0.090 on the basis of 1113 independent reflections. The final atomic coordinates, the thermal parameters, and the lists of the observed and calculated structure factors are deposited as Document No. 72010 at the Office of the Editor of Bull. Chem. Soc. Jpn. The crystal structure of the AsF_6 salt was found to be isostructural to that of the ClO_4 salt[23] with the following crystal data; ($C_8H_4S_8)_3AsF_6(C_2H_3Cl_3$), orthorhombic, space group *Pnma*, a = 12.65(3), b = 35.35(2), c = 10.310(4) Å, V = 4609(10) Å^3, Z = 4, where two independent BMDT-TTF molecules A and B coexist. The bond lengths of BMDT-TTF molecules in this salt shown in Table 1 indicate no appreciable difference between A and B molecules suggesting the presence of negligible if any charge disproportionation between A and B, whereas the bond lengths observed in the ClO_4 salt[23,24] demonstrate a difference in the valence states between A^+ and B^0. The transfer integrals between donor molecules and the energy band structures at room temperature were calculated based on the tight-binding approximation[27] using the extended Hükel Hamiltonian for the $GaCl_4$ salt and the AsF_6 salt.

The susceptibilities were measured using a SQUID magnetometer (Quantum Design, MPMS-5) with about 10 to 20 single crystals (several mg) whose crystal axes were arranged in the same directions using Apiezon N grease. The spin susceptibilities were obtained after the subtraction of the Pascal diamagnetic core con-

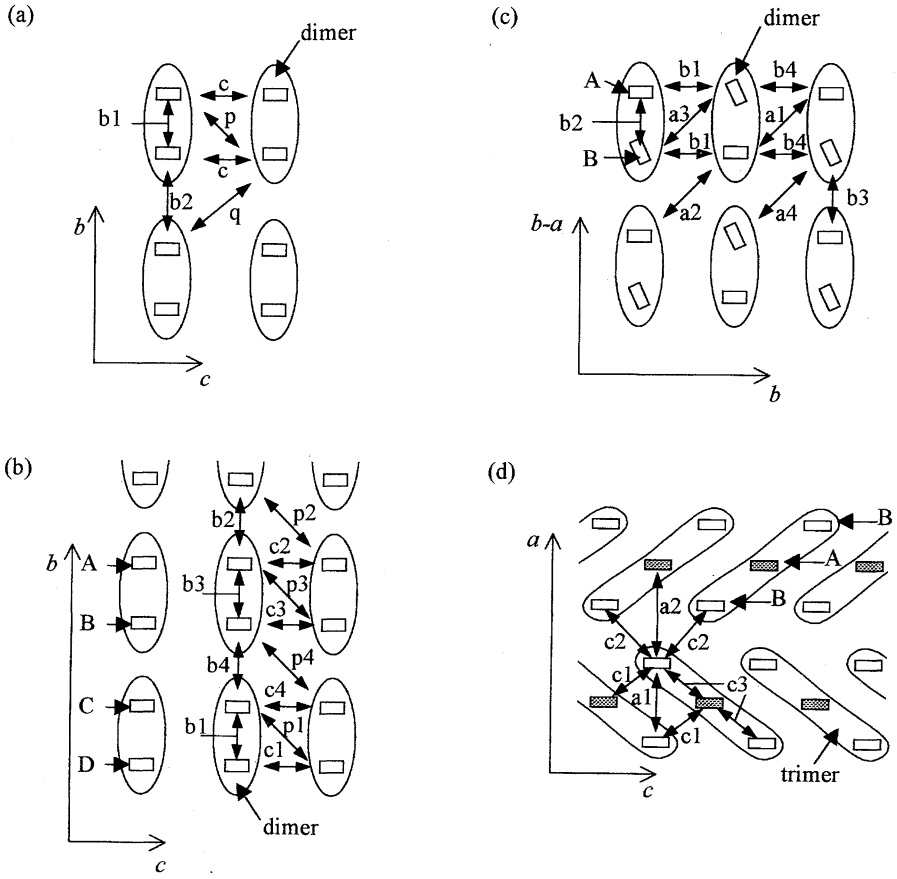

Fig. 2. Schematic structures with inter-molecular transfer integrals in which the crystal structures are simplified to indicate the transfer integrals clearly. A rectangle represents a BEDT-TTF (or BMDT-TTF) molecules viewed along the molecular long axis and an ellipsoid circling two (or three) molecules represents a dimer (or trimer) unit. A and B (and C, D for $(BEDT\text{-}TTF)_2GaCl_4$) indicate the crystallographically independent molecules. (a) β'-$(BEDT\text{-}TTF)_2X$ (X = ICl_2,[16] $AuCl_2$[18]); t_{b1} = 27.2 (26.4), t_{b2} = 10.0 (10.0), t_p = 6.6 (6.5), t_q = −1.6 (−2.0), and t_c = 1.6 (2.3)$\times10^{-2}$ eV for the ICl_2 ($AuCl_2$) salt. (b) $(BEDT\text{-}TTF)_2GaCl_4$; t_{b1} = 22.4, t_{b2} = 3.69, t_{b3} = 26.9, t_{b4} = 3.55, t_{c1} = −0.80, t_{c2} = 2.86, t_{c3} = 2.63, t_{c4} = −4.20, t_{p1} = 8.02, t_{p2} = 1.96, t_{p3} = 5.04, and t_{p4} = 4.71$\times10^{-2}$ eV. (c) α'-$(BEDT\text{-}TTF)_2IBr_2$;[22] t_{a1} = 4.02, t_{a2} = 0.78, t_{a3} = 2.30, t_{a4} = 1.11, t_{b1} = 7.72, t_{b2} = 9.04, t_{b3} = 7.16, and t_{b4} = −5.79$\times10^{-2}$ eV. (d) $(BEDT\text{-}TTF)_2ClO_4$(1,2-dichloroethane)[24] and $(BEDT\text{-}TTF)_2AsF_6$(1,1,2-trichloroethane); t_{a1} = −6.22 (−5.58), t_{a2} = −5.52 (−6.88), t_{c1} = −11.2 (−10.2), t_{c2} = 11.6 (11.0), and t_{c3} = 14.1 (13.7)$\times10^{-2}$ eV for the ClO_4 (AsF_6) salt.

Table 1. Bond Lengths of BMDT-TTF Molecules (A and B Molecules) in $(BMDT\text{-}TTF)_2ClO_4$(1,2-dichloroethane) and $(BMDT\text{-}TTF)_2AsF_6$(1,1,2-trichloroethane)

	a (Å)		*b* (Å)		*c* (Å)		*d* (Å)	
	A	B	A	B	A	B	A	B
$(BMDT\text{-}TTF)_3ClO_4DCE$[a]	1.41	1.35	1.73	1.76	1.73	1.74	1.36	1.32
$(BMDT\text{-}TTF)_3AsF_6TCE$[b]	1.34	1.33	1.75	1.77	1.72	1.74	1.38	1.36

a) Ref. 24, DCE; 1,2-dichloroethane. b) TCE; 1,1,2-trichloroethane.

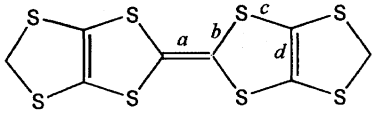

tribution (χ_{dia}), and sometimes, an $S = 1/2$ Curie term associated with a trace of magnetic impurities ($\chi_{impurity}$). Here the estimation gave χ_{dia} = −4.99, −5.06, −5.26, −5.25, −6.34, and −7.17$\times10^{-4}$ emu mol^{-1} for the β'-ICl_2, β'-$AuCl_2$, $GaCl_4$, α'-IBr_2, ClO_4, and AsF_6 salts, respectively. The β'-salts contained no detectable amounts of magnetic impurities, while the other compounds had magnetic impurities of 1.1, 0.54, 2.0, and 1.6% in one formula unit for the $GaCl_4$, α'-IBr_2, ClO_4, and AsF_6 salts, respectively. ESR measurements for the ICl_2 salt and the 3 : 1 salts were carried out with a single crystal, using an X-band ESR spectrometer (JEOL

JES-TE200) with a He cryostat (Oxford ESR910) in the temperature range 4.2—300 K. For the ICl_2 salt, we measured the anisotropy of the resistivity on the *bc*-plane by the Montgomery method[28] to investigate the dimensionality of the β'-salts.

Results

β'-(BEDT-TTF)$_2$X (X = ICl_2, $AuCl_2$). The ratio of the resistivity along the b^*-axis to that along the *c*-axis, is estimated at $\rho_{b*}/\rho_c \approx 0.8$, which is independent of temperature with ρ_c = 20 Ω cm at room temperature. This small anisotropy between the b^*- and *c*-axes indicates the two-dimensionality in the inter-molecular network on the *bc*-plane. The temperature dependence of the susceptibilities[15,29] is shown in Figs. 3(a) and (b) for the ICl_2 and $AuCl_2$ salts, respectively. The susceptibilities have a broad maximum at $T_{max} \approx 110$ K for both salts, which is characteristic of short-range order of a low-dimensional antiferromagnet. There is no observable difference in the data above T_{max} between the two salts, and the fitting to the Curie–Weiss law above 250 K gives a Weiss constant of $\Theta = -140\pm20$ K and a Curie constant of $C = 0.42\pm0.02$ emu mol^{-1} K^{-1} corresponding to the Bohr magneton of $p = 1.83\pm0.05$ per formula unit for both salts, where $p = g\sqrt{S(S+1)} = 1.737-1.740$ for an $S = 1/2$ spin with the observed *g*-value $g = 2.006-2.009$ (see below). The present results of the susceptibility for the ICl_2 salt are qualitatively consistent with the previous reports,[17,21] although the absolute values are not in good quantitative agreement with each other. The data of Ref. 17 are supposed to contain a large error in the absolute value because of the estimation carried out using ESR measurement, while those of Ref. 21 are not treated with the correction of the core diamagnetic susceptibility.

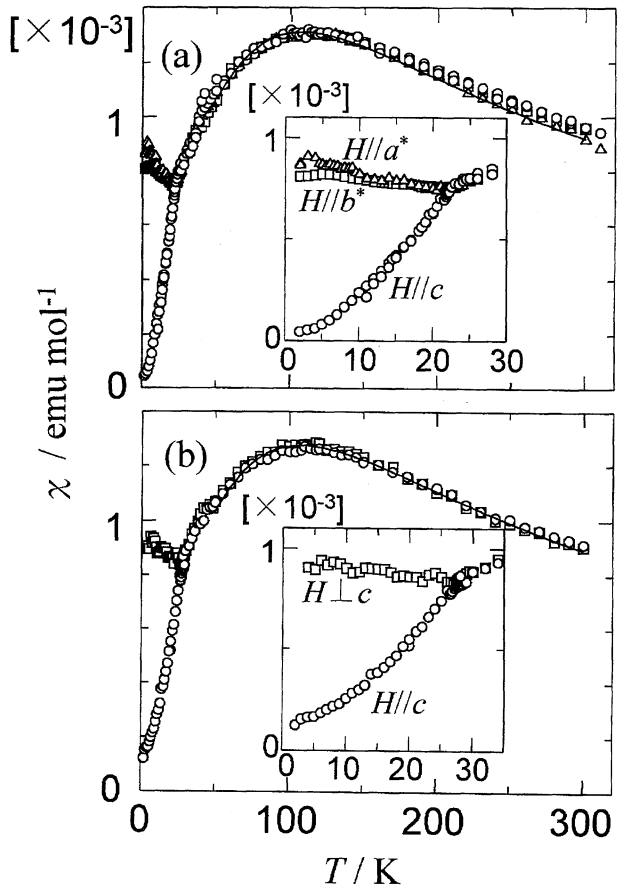

Fig. 3. Temperature dependence of the susceptibility for β'-(BEDT-TTF)$_2$X (X = ICl_2 (a) and $AuCl_2$ (b)) in the applied field parallel to the a^* -(△), b^* -(□), and *c* -(○) axes. The solid curves denote the fittings to the two-dimensional square–lattice $S = 1/2$ Heisenberg antiferromagnet model with $J \approx -59$ K. The insets are the details at low temperatures.

The susceptibilities show discontinuous changes at Néel temperature T_N = 22 and 28 K for the ICl_2 and $AuCl_2$ salts, respectively, indicating the onsets of three-dimensional long-range orderings. From the appearance of anisotropy in the susceptibilities below T_N, we obtain information on the spin easy-axis in the antiferromagnetic ordered state. The susceptibility in the field parallel to the *c*-axis approaches zero as the temperature decreases, suggesting that the easy-axis is oriented to the *c*-axis. The magnetization of the ICl_2 salt at 2 K is shown in Fig. 4 and that of $AuCl_2$ salt (not shown in the Figure) has almost the same behavior. In the magnetization curves, spin flop transitions are observed at H_{sf} = 11 kOe for both salts when the external field is applied parallel to the *c*-axis, in good agreement with the anisotropy in the susceptibilities. The ESR line shape is a Lorentzian-type for the ICl_2 salt. The *g*-values[29] at room temperature are estimated at 2.009, 2.007, and 2.006 for the field parallel to the a^*-, b^*-, and *c*-axes, respectively. The temperature dependence of the line width shown in Fig. 5(a) for the ICl_2 salt is consistent with the previous reports.[17,30] The line width becomes narrow as the temperature decreases accompanied with an upturn below 30 K which becomes divergent as the temperature approaches T_N = 22 K. It is worth noting that the

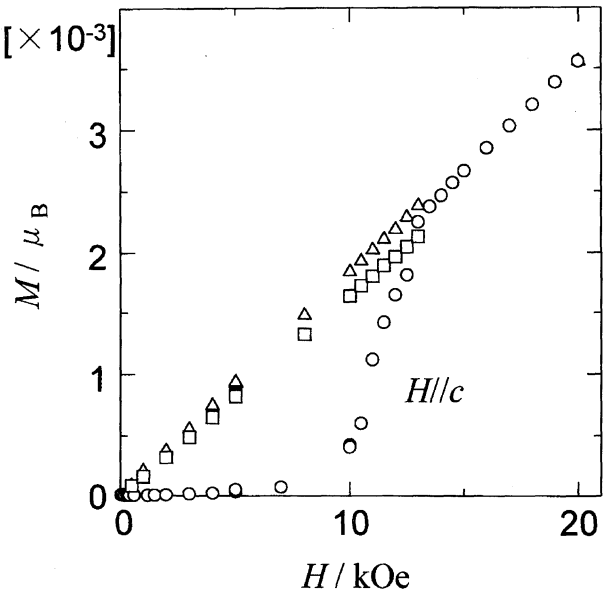

Fig. 4. Magnetization of β'-(BEDT-TTF)$_2$$ICl_2$ at 2 K in the field parallel to the a^* -(△), b^* -(□), and *c* -(○) axes. That of $AuCl_2$ salt shows just the same behavior.

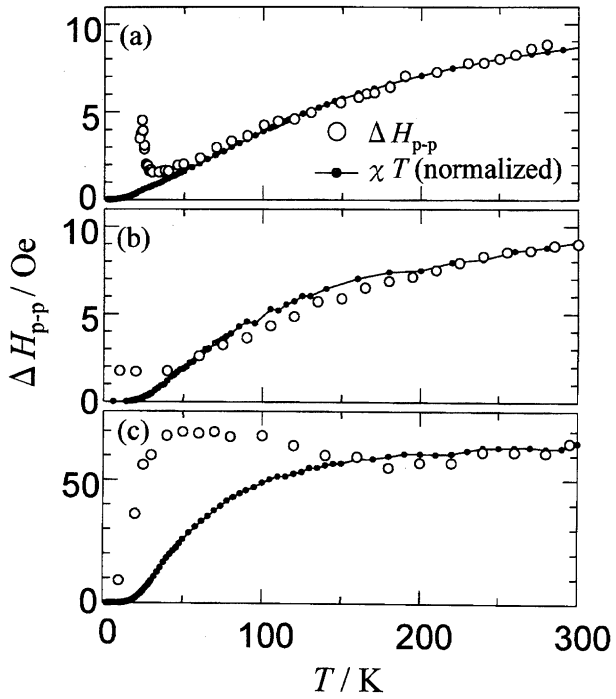

Fig. 5. Temperature dependence of the ESR line widths (open circles) for (a) β'-(BEDT-TTF)$_2$ICl$_2$, (b) (BEDT-TTF)$_2$GaCl$_4$, and (c) α'-(BEDT-TTF)$_2$IBr$_2$ where the data are quoted after Refs. 20 and 30 for the GaCl$_4$ salt and the α'-IBr$_2$ salt, respectively. The experimentally obtained values (closed circles) of χT, which are normalized at room temperature to the line width, are plotted for comparison.

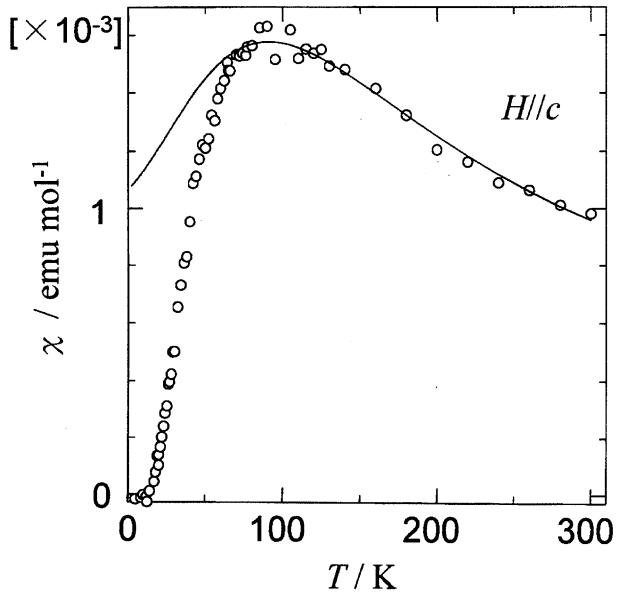

Fig. 6. Temperature dependence of the susceptibility for (BEDT-TTF)$_2$GaCl$_4$ in the applied field parallel to the c-axis. The solid curve is the fitting to the one-dimensional Heisenberg antiferromagnet model with $J \approx -70$ K.

temperature dependence of the line width for the β'-AuCl$_2$ salt[19] is almost the same for the ICl$_2$ salt if the temperature region in which the upturn appears is shifted up while replacing the Néel temperature of 22 K with 28 K.

(BEDT-TTF)$_2$GaCl$_4$. The susceptibility, when the field is parallel to the c-axis, is shown in Fig. 6. The fitting to the Curie–Weiss law gives a Weiss constant of $\Theta = -110\pm20$ K and a Curie constant of $C = 0.40\pm0.02$ emu mol^{-1} K^{-1} (corresponding to the magnetic moment of 1.79 ± 0.05 μ_B per formula unit) above 200 K. The susceptibility shows a broad maximum around 90 K. Then below about 60 K, it approaches zero as $T \rightarrow 0$, which is contradictory to the reported result[20] where it is extrapolated to a finite value (ca. 4×10^{-4} emu mol^{-1}) at 0 K. The presence of magnetic impurities might be considered to cause the wrong result in the previous report. No spin flop transition is observed in the magnetization at 2 K up to 55 kOe. Thus, the magnetic system is suggested to be stabilized in a spin-singlet state at $T = 0$ K.

α'-(BEDT-TTF)$_2$IBr$_2$. Figure 7 shows the temperature dependence of the susceptibility in the field perpendicular to the c^*-axis. The fitting of the susceptibility to the Curie–Weiss law above 150 K shown in the inset of Fig. 7 gives a Weiss constant of $\Theta = -40\pm15$ K and a Curie constant of $C = 0.32\pm0.02$ emu mol^{-1} K^{-1} corresponding to 1.60 ± 0.05 μ_B per formula unit. It has a broad maximum around 60 K and goes to zero independent of the field direction ($H//c^*$ or $H\perp c^*$). Inconsistency in the absolute value of the susceptibility compared with the previous report[21] comes from the same reason for the β'-salt. The magnetization at 2 K does not show any spin flop transition up to 55 kOe. Thus, the magnetic ground state is suggested to be a singlet state.

(BMDT-TTF)$_3$ClO$_4$(1, 2-dichloroethane) and (BMDT-TTF)$_3$AsF$_6$(1,1,2-trichloroethane). The susceptibilities are shown in Fig. 8 for the ClO$_4$ and AsF$_6$ salts.[25] The susceptibilities have almost the same value at room temperature

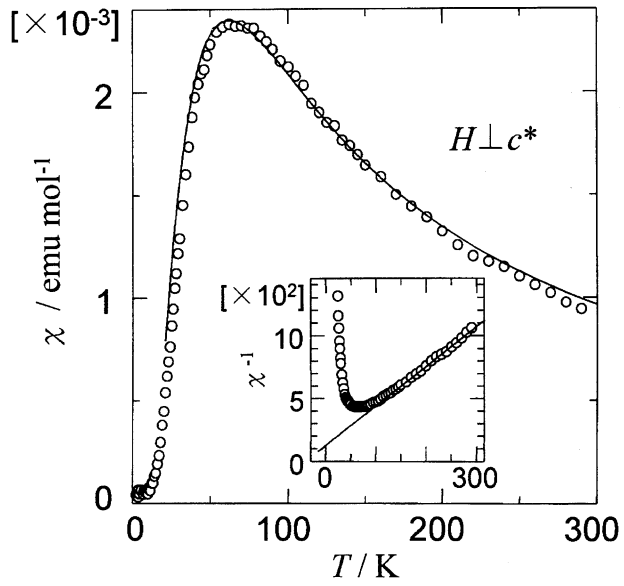

Fig. 7. Temperature dependence of the susceptibility for α'-(BEDT-TTF)$_2$IBr$_2$ in the field perpendicular to the c^*-axis. The solid curve is the fitting to the one-dimensional alternating chain Heisenberg antiferromagnet model with $J \approx -53$ K and $J' \approx -26$ K. The inset is the χ^{-1}–T plot with the fitting curve of the Curie–Weiss law ($\Theta = -40$ K).

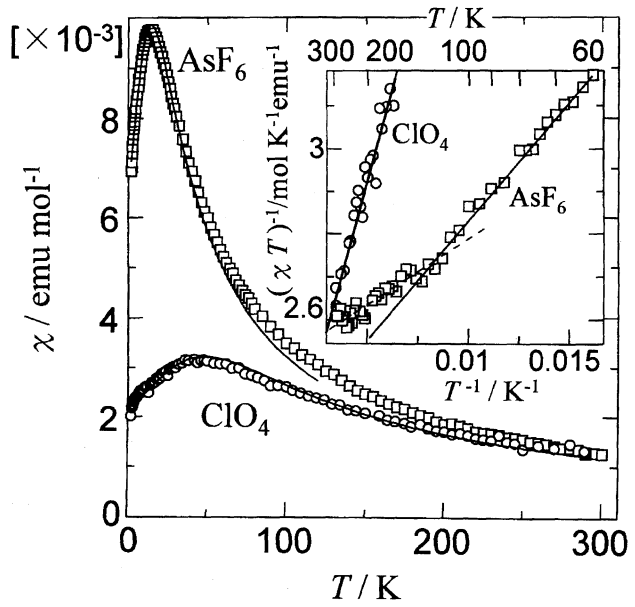

Fig. 8. Temperature dependence of the susceptibilities for $(BMDT\text{-}TTF)_2ClO_4$(1,2-dichloroethane) and $(BMDT\text{-}TTF)_2AsF_6$(1,1,2-trichloroethane) with the fittings to the one-dimensional Heisenberg antiferromagnet model with $J \approx -37$ K and -11 K for the ClO_4 and AsF_6 salts, respectively. The inset is the $(\chi T)^{-1}$ vs. T^{-1} plot for both salts, where the lines are the Curie–Weiss fittings with $\Theta = -50$ K for the ClO_4 salts, $\Theta = -15$ K (dashed line above 150 K) and -23 K (solid line below 150 K) for the AsF_6 salt, respectively.

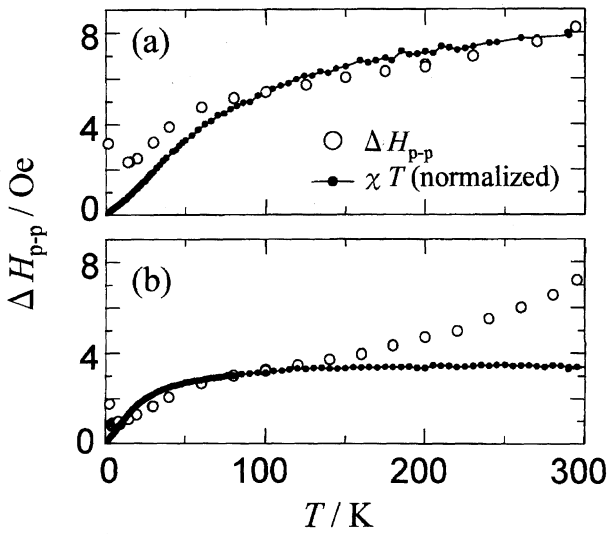

Fig. 9. The temperature dependence of the ESR line widths (open circles) for (a) $(BMDT\text{-}TTF)_3ClO_4$(1,2-dichloroethane) and (b) $(BMDT\text{-}TTF)_3AsF_6$(1,1,2-trichloroethane). The normalized χT are plotted (closed circles), where the line widths at room temperature and 100 K are taken as references for the ClO_4 and AsF_6 salts, respectively.

(ca. 1.2×10^{-3} emu mol^{-1}) for both salts, whereas they gradually deviate from each other as the temperature decreases. The susceptibility of the ClO_4 salt obeys the Curie–Weiss law with a Weiss constant of $\Theta = -50\pm10$ K and a Curie constant of $C = 0.43\pm0.02$ emu mol^{-1} K^{-1} corresponding to 1.85 ± 0.05 μ_B per formula unit above 150 K. Meanwhile, the data of the AsF_6 salt show a change in both the Weiss constant and the Curie constant around 150 K as shown in the inset of Fig. 8, obviously indicated by the $(\chi T)^{-1}$ vs. T^{-1} plot. The fitting of the data to the Curie–Weiss law gives a Weiss constant of $\Theta = -15\pm3$ K and a Curie constant of $C = 0.40\pm0.02$ emu mol^{-1} K^{-1} corresponding to 1.79 ± 0.05 μ_B above 150 K (dotted line) and $\Theta = -23\pm1$ K and $C = 0.42\pm0.01$ emu mol^{-1} K^{-1} (1.83 ± 0.02 μ_B) between 50 and 150 K (solid line) for the AsF_6 salt. In much lower temperature range, a broad maximum emerges around 40 and 12 K for the ClO_4 and AsF_6 salts, respectively, suggesting the behavior of short-range ordering. No antiferromagnetic transition is observed, not only in the temperature dependence of the susceptibility but also in the magnetization up to 50 kOe at 2 K for both salts. The ESR g-values at room temperature are estimated at 2.003, 2.014, and 2.005, in the fields parallel to the a-, b-, and c-axes, respectively, for both salts. The ESR line widths for both salts are almost the same value of about 8 Oe ($H//c$) at room temperature with Lorentzian-type line shapes. The temperature dependence of the line widths shown in Fig. 9 is different from each other. In the ClO_4 salt, the line width decreases moderately in the high temperature range above 50 K as the temperature is lowered, and then it shows a steep decrease below ca. 50 K, which is followed by an upturn appearing below 10 K. The line width of the AsF_6 salt becomes much narrower than that of the ClO_4 salt at low temperatures. There is an inflection point in the ΔH_{p-p} vs. T plot at 150 K, at which the discontinuous change in the susceptibility emerges.

Discussion

Quasi- Two- Dimensional Antiferromagnetic (AF) Structure of the β'-Salts. For the consideration of the magnetic structure, we reexamine the structural feature of BEDT-TTF molecules in the β'-salts using a schematic structure depicted in Fig. 2(a), where the triclinic structures are simplified to indicate the paths of the transfer integrals clearly. Since the largest transfer integral t_{b1} is more than 2 times larger than the other transfer integrals, BEDT-TTF molecules are strongly dimerized by face-to-face contact t_{b1} in the bc-plane, where the b-axis is the stacking direction of dimerized molecules while the c-axis corresponds with the side-by-side direction. The charge neutrality rule in addition to the 2 : 1 composition ratio requires the presence of a hole per donor dimer, so that each dimer is considered to possess an $S = 1/2$ spin. The spins on the dimers interact with each other through the inter-dimer exchange interactions which are related to the corresponding inter-dimer transfer integrals. If one takes into account that the exchange interaction J is described in terms of the transfer integral t and the on-site Coulomb interaction U as $J \approx -t^2/U$,[15] the estimation of the ratio of the interaction along the b-axis to that along the c-axis is given by $J_b/J_c = (|t_{b2}|)^2/(|t_c|+|t_c|+|t_p|)^2 \approx 1.0$ and ≈ 0.81 for the ICl_2 and $AuCl_2$ salts, respectively. Consequently, the

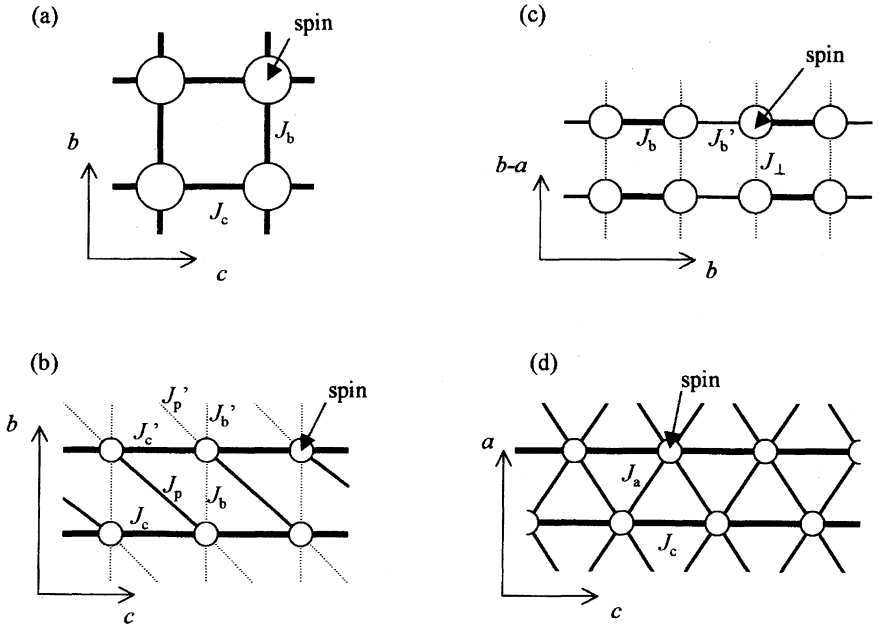

Fig. 10. Magnetic structures predicted from Fig. 2. A circle represents a magnetic unit and a line linking the circles represents an exchange interaction J, where the strengths of the interactions are on the order of bold solid line > thin solid line > dotted line. (a) β'-(BEDT-TTF)$_2$X (X = ICl_2, $AuCl_2$). (b) (BEDT-TTF)$_2GaCl_4$. (c) α'-(BEDT-TTF)$_2IBr_2$. (d) (BMDT-TTF)$_2ClO_4$(1,2-dichloroethane), and (BMDT-TTF)$_2AsF_6$(1,1,2-trichloroethane).

magnetic structure features a quasi-two-dimensional square-lattice network in the bc-plane, as shown in Fig. 10(a), taking account of the small value of the second nearest neighbor interaction corresponding to t_q. The small anisotropy of the resistivity in the bc-plane on which donor molecules form a two-dimensional layer, demonstrates quasi-two-dimensionality in the electronic structure for the β'-salt, while the band structure[16,18] is effectively half-filled with a one-dimensional Fermi surface because of the influence of the strong dimerization. The Bohr magneton per dimer unit is estimated at 1.83±0.05 from the fitting to the Curie–Weiss law for both salts, indicating the existence of an $S = 1/2$ localized spin per dimer unit. (The expected magnetic moment for $S = 1/2$ with $g = 2.0023$ is given to be 1.73 μ_B. The overestimation of the magnetic moment by ca. 0.1 μ_B can be explained as due the inaccuracy in the subtraction of the diamagnetic core susceptibility from the observed susceptibility. We will comment on the overestimation in a later section.)

The strength of the intra-layer exchange interaction can be estimated on the basis of the two-dimensional square-lattice Heisenberg antiferromagnet model[31] if we neglect the difference between J_b and J_c. The fitting of the susceptibility vs temperature plot to the model gives J (= $J_b \approx J_c$) ≈ -59 K for both ICl_2 and $AuCl_2$ salts, as shown in Fig. 3. The estimation of the intra-layer interaction is possible also using the value of the perpendicular susceptibility at 0 K, $\chi_\perp(0)$. According to the spin wave theory,[32] $\chi_\perp(0)$ is expressed as

$$\chi_\perp(0) \approx \chi_\perp^0 \left[1 - \Delta S/S - e(0)/2zS\right], \quad (1)$$

for a two-dimensional square-lattice system when $H_A \ll H_E$ where H_A is the magnetic anisotropy field and H_E is the exchange field. $\chi_\perp^0$ is the temperature-independent perpendicular susceptibility based on the molecular field theory, $\chi_\perp^0 = Ng^2\mu_B^2/4zJ$, z is the number of the nearest neighbors, $\Delta S/S$ is the spin reduction term for the sublattice magnetization, and $e(0)/2zS$ is the correction for the real ground state spin energy. The estimation[29] based on Eq. 1 gives a value of the intra-layer exchange interaction $J \approx -50$ K for both salts using the values of $\Delta S/S = 0.394$,[32] $e(0) = 0.632$,[32] $z = 4$, and the experimental values of $\chi_\perp(0) \approx 0.9\times10^{-3}$ emu mol^{-1} from Fig. 3, in good quantitative agreement with $J \approx -59$ K estimated from the high temperature region.

Next, we discuss the spin flop transition field H_{sf} which is expressed as $H_{sf} = \sqrt{2H_A \cdot H_E}$ on the basis of the molecular field approximation sufficiently below T_N. We obtain the ratio $H_A/H_E \approx 2.0\times10^{-5}$ and then $H_A \approx 3$ mK using the observed values of $H_{sf} = 11$ kOe and $H_E = 2zJS/g\mu_B \approx 1.75$ MOe where we employ $J \approx -59$ K and $g = 2.006$ estimated from ESR for both salts. This value of H_A is in good agreement with that obtained in the antiferromagnetic resonance measurements (H_A = 7—14 mK)[33] which originates mainly from the dipole–dipole interaction. The difference in the Néel temperatures between the two salts (22 K for the ICl_2 salt and 28 K for the $AuCl_2$ salt) is considered to be caused by the difference in the inter-layer exchange interaction J'. The Green function method[34] is available for the estimation of the inter-layer exchange interaction in an $S = 1/2$ quasi-two-dimensional square-lattice system:

$$\frac{J}{k_B T_N} = \frac{1}{\pi^3}\int\int_0^\pi\int \frac{dq_x dq_y dq_z}{(1-\cos q_x)+(1-\cos q_y)+\eta(1-\cos q_z)}, \quad (2)$$

where q_i ($i = x$, y, and z) is the component of a wave number vector q, and $\eta = J'/J$. Equation 2 gives $J'/J \approx 1\times10^{-4}$ for the ICl_2 salt and 1×10^{-3} for the $AuCl_2$ salt, respectively, us-

Table 2. Cell Constants of β'-(BEDT-TTF)$_2$X (X = ICl_2, $AuCl_2$) after Refs. 16 and 18
$\Delta l/l$ is the relative difference in the cell constant of the $AuCl_2$ salt from that of the ICl_2 salt.

	a (inter-layer)	*b* (intra-layer)	*c* (intra-layer)
X=ICl_2[a] (Å)	12.937	9.778	6.636
X=$AuCl_2$[b] (Å)	12.766	9.763	6.640
$\Delta l/l$ (l=a, b, c) (%)	1.32	0.15	−0.06

a) Ref. 16. b) Ref. 18.

ing the value of the intra-layer exchange interaction $J \approx -59$ K and the observed values of the Néel temperatures.[29] The origin of the large difference in the inter-layer exchange interactions between the two salts is reasonably understood from the difference in the layer stacking structure between the large ICl_2^- and small $AuCl_2^-$ anions. There is almost no difference in the cell constants for the *b*- and *c*-axes between the two salts, as shown in Table 2, which is consistent with the value of the intra-layer exchange interaction J (≈ -59 K) between the two salts. In the meantime, the difference in the cell constants for the *a*-axis corresponding to the inter-layer distances is one order of magnitude larger than that in the *b*- or *c*-axis. Hence, the difference in T_N between the two salts is suggested to be caused by the difference in the inter-layer distances, implying that the inter-layer interaction (J') originates from exchange interactions since only a small change in the lattice constant ranging ca. 1% varies the strength of the interaction by one order of magnitude.

Two-Leg-Ladder Antiferromagnet of the $GaCl_4$ Salt. The crystal structure of the $GaCl_4$ salt[20] shown in Fig. 2(b) contains two kinds of dimer units consisting of molecules A–B and C–D coupled through the intra-dimer transfer integrals $t_{intra} = t_{b3}$ and t_{b1}, respectively. Strong dimerization, which is evidenced by the large intra- to inter-dimer transfer integral ratios $t_{b3}/t_{p3} = 5.3$ and $t_{b1}/t_{p1} = 2.8$, produces an effectively half-filled band structure similar to that of the β'-salts. The Bohr magneton of 1.79 per formula unit, thus, indicates that one localized electron is allotted to a dimer unit. From the crystal structure of the $GaCl_4$ salt, the magnetic structure can be predicted along the same way as the β'-salts, as exhibited in Fig. 2(b). The dimers form two kinds of one-dimensional chains along the *c*-axis through J_c (consisting of the inter-dimer transfer integrals t_{c4}, t_{c1}, and t_{p1}) and J_c' (t_{c2}, t_{c3}, and t_{p3}) where the ratio of the strengths is estimated at $J_c'/J_c \approx 0.65$. There are four kinds of inter-chain interactions, J_p (t_{p4}), $J_p'(t_{p2})$, $J_b(t_{b4})$, and $J_b'(t_{b2})$, whose strengths are estimated at $J_p \approx 0.13\ J_c$, $J_b \approx 0.07\ J_c$, $J_p' \approx 0.02\ J_c$, and $J_b' \approx 0.08\ J_c$. Thus, the $GaCl_4$ salt forms a quasi-one-dimensional structure with alternating inter-chain interactions as shown in Fig. 10(b). Here, if we neglect the second nearest and further inter-chain interactions, the magnetic lattice can be approximated to a two-leg-ladder structure similar to λ-(BETS)$_2$GaX$_z$Y$_{4-z}$ (X, Y = F, Cl, Br).[35] To estimate the exchange interaction, we first employ the one-dimensional Heisenberg antiferromagnet model[36] while neglecting all the inter-chain interactions. The fitting with this model for the temperature dependence of the susceptibility gives the intra-chain exchange interaction $J \approx -70$ K (solid curve in Fig. 6) above the temperature at which a susceptibility hump appears, while the fitting curve deviates from the experimental result below 60 K approaching zero as $T \rightarrow 0$ K. Although the previous report[20] suggests the presence of a three-dimensional antiferromagnetic ordering based on the finite susceptibility extrapolated to 0 K (ca. 4×10^{-4} emu mol^{-1}), it is doubtful due to the serious influence of magnetic impurities at low temperatures. Our result clearly reveals that the magnetic ground state is the spin-singlet one, suggesting the importance of the alternation in the strengths of the inter-chain exchange interactions, since a spin gap is opened in one-dimensional chains connected by alternating inter-chain interaction whose extreme is characterized as a two-leg-ladder system. Therefore, not only the β'-salts but the $GaCl_4$ salt can be described as a strong dimerization system, where the absence of three-dimensional long-range order in the $GaCl_4$ salt is considered to be associated with the specific exchange interaction network of a spin-ladder system, in contrast with the three-dimensional antiferromagnetic ordering of the β'-salts.

Quasi-One-Dimensional Alternating Chain AF Structure of the α'-IBr_2 Salt. In contrast with the β'-salts and the $GaCl_4$ salt, the degree of dimerization is very weak in the α'-salt[22] which consists of two independent molecules A and B, since the largest transfer integral (t_{b2}) is only 17% larger than the second largest one (t_{b1}), as shown in Fig. 2(c). Consequently, the intra-dimer transfer integral is not large enough to open a gap between the upper and lower bands. In other words, the 3/4-filled band structure does not form an effectively half-filled band different from that of the β'-salts, and thus this compound is not a simple Mott insulator. This means that electrons are not well localized in the dimers, that is, electrons are delocalized to some extent as evidenced by the low resistivity[21] ranging ca. 0.5 Ω cm at room temperature. The fractional magnetic moment, which is evidenced by a small Bohr magneton of 1.60±0.05 per formula unit compared with that expected for $S = 1/2$, is favorable to the feature of the delocalized electronic structure. Here, we treat the experimental results on the basis of the localized electron model in order to see the statistical dynamics behavior of the magnetic system, although the employment of the itinerant electron model would seem to be more appropriate. The dimer units are networked as shown in Fig. 2(c) mainly through t_{b1}, t_{b3}, t_{b4}, and t_{a1}; the strongest inter-dimer interaction J_b consists of t_{b1} and t_{a3}, and the second strongest one J_b' consists of t_{b4} and t_{a1}, where the estimation gives $J_b'/J_b \approx 0.77$. The inter-chain interaction $J_\perp$ is estimated at $J_\perp \approx 0.16\ J_b$ where we take only t_{b3} as

the main contributor to $J_\perp$. Therefore, a quasi-one-dimensional alternating chain structure is formed along the *b*-axis, as shown in Fig. 10(c). The broad peak of the susceptibility is explained by the one-dimensional chain model with the alternating exchange interactions[37] J and J' where the fitting of the data gives $J \approx -53$ K and $J' \approx -26$ K ($J'/J \approx 0.5$). The estimated ratio of J'/J is in roughly quantitative agreement with that calculated from the transfer integrals. The absence of three-dimensional long-range ordering in the α'-IBr_2 salts can be explained as associated with the alternation in the strengths of the intra-chain exchange interactions along the *b*-axis, which brings about the dimerization of the spins sitting on two adjacent dimer units.

Quasi-One-Dimensional AF Structure with Frustration Effect in the 3 : 1 Salts. The schematic structure is shown in Fig. 2(d) for the ClO_4[23,24] and AsF_6[25] salts which contains two independent BMDT-TTF molecules A and B on the *ac*-plane. The largest transfer integral t_{c3}, which is only 22 and 25% larger than the second largest one t_{c2}, for the ClO_4 and AsF_6 salts, respectively, gives weakly trimerized units comprising one A molecule and two B molecules. The intra-trimer interaction comparable to the inter-trimer interaction seems to bring some inappropriateness in the treatment with a trimer-based system; however, we will try to explain the magnetic structure based on the trimer unit. The band structure is described in terms of the 5/6-filled band with the coexistence of a one-dimensional Fermi surface along the *c*-axis and a two-dimensional Fermi surface on the *ac*-plane. The weakness of the trimerization seems not to give an effectively half-filled band, suggesting a deviation from a simple Mott insulator system, similar to the α'-salt having small fractional magnetic moments. On the contrary, the experimental finding that the 3 : 1 salts have the magnetic moment of about 1.8 μ_B per formula unit indicates the localization of an electron within a trimer. One clue to achieve more consistency between the opposite trends consists in describing a specific charge distribution in the donor network. The crystal structure analysis[23,24] proves the presence of charge disproportionation between A^+ and B^0 donor molecules in the ClO_4 salt. This means that the inter-site Coulomb interaction works to make electrons apart from each other to achieve the energy stabilization, as discussed in the previous report.[24] Therefore, the contribution of the inter-site Coulomb interaction allows us to treat the ClO_4 salt as a localized spin system. In the meantime, the AsF_6 salt has no charge disproportionation between the two independent donors A and B, suggesting the delocalization of charges among donors in a trimer unit which is favorable to the experimental finding in the ESR spectra as discussed in the later section. The observed value ca. 1.8 μ_B of the magnetic moment per trimer seems to be inconsistent with such delocalized electronic features. However, there is a suggestive feature related to an electron delocalization-to-localization change in the susceptibility. The AsF_6 salt undergoes successive phase transitions around 150 K and ca. 200—290 K with a large hysteresis from a high-temperature conductive state to a low-temperature less conductive state, where the application of pressure makes the high temperature phase metallic.[25] The behavior of the susceptibility shown in the inset of Fig. 8 reflects the transition, as evidenced by the presence of a kink in the Curie–Weiss plot. As shown in Fig. 8, the magnetic moment above the phase transition at $T_c \approx 150$ K is about 2% smaller than that below T_c, the latter of which has the same value as the magnetic moment of the ClO_4 salt.

The reduced magnetic moment above T_c is considered to be associated with the delocalized feature of the electrons. Taking into account the importance of the inter-site Coulomb interaction in the ClO_4 salt, the AsF_6 salt, which has the same crystal structure, is expected to play a similar role of the inter-site Coulomb interaction, especially, in the low temperature phase, which eventually makes electrons localized within trimers similar to the ClO_4 salt.

We discuss the magnetic structure on the basis of the localized spin model, in which the crystal structure at room temperature is taken into account. Considering a trimer as a magnetic unit, the trimers interact with each other along the *c*-axis through J_c (consisting of t_{c1} and t_{a1}) and then along the *a*-axis through J_a (t_{c2} and t_{a2}) where $J_a/J_c \approx (|t_{a2}|+|t_{c2}|)^2/(|t_{c1}|+|t_{a1}|+|t_{c1}|)^2 \approx 0.36$ and 0.47 for the ClO_4 and AsF_6 salts, respectively. Accordingly, the structural feature based on the trimer unit is described as the J_c-dominated one-dimensional chain structure with inter-chain interactions J_a as shown in Fig. 10(d) where the participation of J_a adds a frustration feature to the exchange interaction network. In the ClO_4 salt, the fitting of the susceptibility to the $S = 1/2$ one-dimensional Heisenberg antiferromagnet model[36] gives the exchange interaction $J \approx -37$ K over the whole temperature range measured, as shown in Fig. 8, with neglecting the contribution of J_a. The absence of an antiferromagnetic transition observed for the ClO_4 salt is caused by the frustration introduced by the strong inter-chain exchange interactions. For the AsF_6 salt, a similar estimate of the exchange interaction[36] gives $J \approx -11$ K in the temperature range between 2 and 60 K. Thus, the experimental results indicate a large difference in the exchange interactions between the two salts. The phase transition at $T_c \approx 150$ K, which makes the value of the magnetic moment increase to that expected for an $S = 1/2$ per trimer below T_c, is considered to result in the localization of the electrons, reducing the inter-trimer transfer integrals and eventually the strengths of the exchange interactions, although the crystal structure analysis in the low temperature range is required for a final conclusion.

ESR Line Width and the Electron Localization. The ESR line width is a good indicator for characterizing the magnetic structure and the electron transport process. The spin–spin relaxation, which is one of the origins of the ESR line width, is governed by the dipole–dipole interaction, where the line width associated with this process is subjected to the exchange-narrowing mechanism in an exchange-interaction-networked localized spin system. Meanwhile, the contribution of the spin–lattice relaxation becomes dominant in the line width of the delocalized electron system, which is related to the relaxation time of carriers in the conduc-

tion process, since the rapid motion of the carriers makes the width of the spin–spin relaxation completely disappear due to the motional narrowing process. Actually, in most metallic charge transfer salts which have ever been investigated,[8,11,38] the line width is predominated by the spin–lattice relaxation process of carriers, while complexes in the localized regime make an important contribution of the spin–spin relaxation to the line width, as will be shown in this section. Here, we investigate the feature of the ESR line width in relation to the strength of dimerization/trimerization of donors, which is considered to be responsible for the electron localization.

First we discuss the correlation between the line width and the degree of electron delocalization in the 2 : 1 salts. The β'-ICl_2 salt and the $GaCl_4$ salt,[20] which are typical strong dimerization systems, have narrow ESR line widths of ca. 10 Oe at room temperature. The well localized electronic structures of these salts are characterized to be Mott insulators as evidenced by the poor electrical conductivity ($\sigma \approx 0.05$—$0.1\ S\,cm^{-1}$) and the less temperature dependent large thermoelectric powers ranging from 100 to 400 $\mu V\,K^{-1}$ at room temperature.[39,40] Figure 5 shows the correlation between the line width and the χT product,[20,30] based on the spin-diffusion theory of the spin–spin relaxation mechanism in the low-dimensional magnets[41] where the combination of the dipole–dipole and exchange interactions makes the line width proportional to χT at high temperatures above the temperature at which the thermal energy becomes comparable to the exchange interaction. The temperature dependence of the line widths for the β'-ICl_2 salt and the $GaCl_4$ salt have almost the same behavior as that of the χT products, which means that the dipole–dipole interaction and the exchange interaction related to the χT product play the major roles in the behavior of the line width. Thus, this ESR behavior of the salts having strong dimerization suggests self-consistency between the localized spin feature in the magnetic structure and their spin dynamics. On the other hand, the α'-IBr_2 salt having less dimerized structural features[22] is a great contrast to the β'-salts and the $GaCl_4$ salt. The delocalized electronic feature in the α'-salt is obvious from the low resistivity ca. 0.5 $\Omega\,cm$[21] and the small thermoelectric power ca. +25 $\mu V\,K^{-1}$.[39] Its remarkably broad line width ca. 60 Oe[30] is in the similar range to that of typical metallic BEDT-TTF complexes,[8,11,38] and the temperature dependence of the line width[30] shown in Fig. 5(c) reveals a considerable difference from that of the χT product. Actually, a large deviation appears at lower temperatures though the χT product seems to be similar to that of the line width above ca. 150 K except for the broadness of the line width. As a consequence it is suggested that the line width of the α'-salt is strongly influenced by the spin–lattice relaxation process. These features in the α'-salt with weak dimerization are considered to be generated by the delocalization of the electrons, giving a contribution of the spin–lattice relaxation to the line width similar to the case of metallic compounds.

The ESR line width in the 3 : 1 salts is suggestive from the viewpoint of electron localization/delocalization. Figure 9 shows the temperature dependence of the line width for the 3 : 1 salts in comparison with the χT product. There is a large difference in the behavior of the temperature dependence of the ESR line width between the ClO_4 and AsF_6 salts, whereas the absolute values of ca. 10 Oe are in the same range to those of the localized spin systems of the 2 : 1 salts. The line width in the ClO_4 salt is subjected to the spin–spin relaxation process, as suggested by the similarity in the temperature dependence between the line width and χT, which is a good indication that the spin system has a well localized feature. The behavior of the AsF_6 salt is not explained simply by the feature of the localized spin system, especially the behavior in the high temperature phase above $T_c \approx 150$ K. Namely, the temperature dependence above T_c seems to have an additional contribution, although the line width has the similar temperature dependence to that of χT below T_c. Taking account of the delocalized feature of the electrons in the trimer for the AsF_6 salt, which is deduced from the room temperature crystal structure, the additional contribution is considered to reflect the spin–lattice relaxation process of the mobile π-electrons. This is consistent with the change in the value of the magnetic moment at T_c.

Strength of Dimerization/Trimerization and Magnetic Interaction. In the previous sections, we discussed four kinds of the magnetic structures and the feature of the ESR line width on the basis of a dimer/trimer unit to which an $S = 1/2$ spin is allotted. From the structural aspect, the β'-salts and the $GaCl_4$ salt are characterized well in terms of strong dimerization, in contrast with the other three salts where the dimer/trimer model is not so appropriate. Nevertheless, the dimer/trimer-based magnetic structures well explain the experimental results for all the salts investigated, which indicates the validity of the employed model, especially from the viewpoint of statistical mechanics of localized spin systems. To see more details in the difference between the salts with strong and weak dimerization/trimerization, we discuss the relationship between the exchange interactions and the transfer integrals. Table 3 summarizes the exchange interactions, the Weiss constants and the representative transfer integrals for all the salts investigated. Here, J_{exp} and Θ_{exp} are the exchange interactions estimated from the low-dimensional magnet models and the Weiss constants estimated experimentally, respectively. Θ_{MF} is calculated from $\Theta_{MF} = (1/2)\sum J_{exp}$ on the basis of the molecular field theory with $S = 1/2$ where the summation is carried out over all the nearest neighbor spins, as shown in Fig. 10. The obtained values of Θ_{MF} are in good agreement with the experimental data, Θ_{exp}, suggesting the appropriateness of the data treatments at high temperatures. t_{intra} is the intra-dimer/trimer transfer integrals. Here, we introduce t_{eff} as a parameter representing an effective transfer integral between two adjacent spins in the expression of the exchange interaction between the dimer/trimer units given by $J \approx -t_{eff}^2/U_{eff}$ where U_{eff} is the effective on-site Coulomb interaction on a dimer/trimer unit. U_{eff} in the dimer-based systems is obtained from the following equation:[15]

Table 3. Exchange Interactions, Weiss Constants, and Transfer Integrals
J_{exp}; the exchange interactions obtained from the models (see the text), Θ_{exp}; the experimental Weiss constants, Θ_{MF}; the calculated Weiss constants from J_{exp} in the molecular field theory, t_{intra}; the intra-dimer (trimer) transfer integrals estimated from the overlap integrals, t_{eff}; the inter-dimer (trimer) transfer integrals estimated from J_{exp}, p; the Bohr magnetons per dimer/trimer unit.
$(BEDT\text{-}TTF)_2GaCl_4$ has two kinds of the t_{intra} and t_{eff} for two independent dimer units.

	J_{exp}	Θ_{exp}	Θ_{MF}	t_{intra}	t_{eff}	P
	K	K	K	eV	eV	
β'-$(BEDT\text{-}TTF)_2ICl_2$	−59	−140±20	−118	0.272	0.052	1.83±0.05
$(BEDT\text{-}TTF)_2GaCl_4$	−70	−110±20	−70	0.269 0.224	0.057 0.052	1.79±0.05
α'-$(BEDT\text{-}TTF)_2IBr_2$	−53	−40±15	−40	0.090	0.028	1.60±0.05
$(BMDT\text{-}TTF)_3ClO_4DCE$[a]	−37	−50±10	−37	0.141	0.025	1.85±0.05
$(BMDT\text{-}TTF)_3AsF_6TCE$[b] ($T>150$ K)	—	−15±3	—	0.137	—	1.79±0.05
($2<T<150$ K)	−11	−23±1	−11	—	—	1.83±0.02

a) DCE; 1,2-dichloroethane. b) TCE; 1,1,2-trichloroethane.

$$U_{eff} = 2\,|\,t_{intra}\,| + \left[U_0 - \sqrt{{U_0}^2 + 16{t_{intra}}^2}\right]/2, \quad (3)$$

which is approximated to $U_{eff} \approx 2|t_{intra}|$ in charge transfer salts with strongly dimerized donor structure, since the on-site Coulomb interaction for a molecule U_0 (ca. 1—2 eV) is one order of magnitude larger than the intra-dimer transfer integral t_{intra} (ca. 0.1—0.3 eV). The expression of U_{eff} for the trimer system,[42] which is obtained by an equation similar to Eq. 3, leads to $U_{eff} \approx \sqrt{2}|t_{intra}|$ for strong trimerization. Thus, we obtain $t_{eff} \approx \sqrt{2|J_{exp}|\cdot|t_{intra}|/\xi}$ as an estimation of the effective t_{inter} working between adjacent spins, as summarized in Table 3, where $\xi = 1$ and $\sqrt{2}$ for dimerized and trimerized systems, respectively. It is worth noting that the above treatment with t_{eff} is valid only for the case where a dimerized/trimerized unit is well defined; that is, the intra-dimer/trimer transfer integral is required to be considerably larger than the inter-dimer/trimer transfer integral. From this aspect, the estimated values t_{eff} well reflect the strength of dimerization/trimerization as revealed in Table 3. Namely, there is a good correlation between the experimentally obtained Weiss temperatures and the values of t_{eff} in the β'-salts and the $GaCl_4$ salt having strong dimerization. On the contrary, the α'-salt has a smaller t_{eff} than that expected in the case of strong dimerization. Consequently, the diagnosis on the basis of the treatment with transfer integrals t_{eff} gives additional information on the deviation from the purely localized spin model treated by statistical dynamics for the weakly dimerized systems.

The most important feature of the salts investigated in this paper is reflected in the values of the magnetic moments, as summarized in Table 3. The magnetic moments of the salts except the α'-IBr_2 salt have larger values than the expected value of 1.73 μ_B for $S = 1/2$ by about 0.1 μ_B. This might be associated with the systematic errors coming from the core diamagnetic contributions we employ for the corrections of the core diamagnetism. Assuming that the 0.1 μ_B excess can be subtracted commonly from the observed values of the magnetic moments as an artificially added contribution, one may conclude that the magnetic moment for the α'-salt has a smaller magnetic moment ca. 1.5 μ_B than that expected for $S = 1/2$ due to the electron delocalization. The reduction of the magnetic moment in the high temperature conductive phase on the AsF_6 salt ($T > 150$ K) is suggestive as well from the point of the electron delocalization.

Conclusion

We investigated the magnetic properties of several TTF-based charge transfer salts in the Mott insulator regime consisting of dimerized/trimerized-donor units, which are classified into three subgroups: (1) β'-$(BEDT\text{-}TTF)_2X$ ($X = ICl_2$, $AuCl_2$) and $(BEDT\text{-}TTF)_2GaCl_4$ as strong dimer systems, (2) α'-$(BEDT\text{-}TTF)_2IBr_2$ salt as a weak dimer system, and (3) $(BMDT\text{-}TTF)_3ClO_4$(1,2-dichloroethane) and $(BMDT\text{-}TTF)_3AsF_6$(1,1,2-trichloroethane) as weak trimer systems. Group (1) is considered to be the typical Mott insulators; to this group belong most of the charge transfer salts having strongly dimerized donor structures. Groups (2) and (3) are situated in the marginal region of the Mott insulator group, where weak dimerization/trimerization in the crystal structures adds some electron delocalization features. Groups (1)—(3) cover almost the whole Mott insulator region in Fig. 1 except the bounding to the metal region where well-known $\varkappa$-type BEDT-TTF salts are located. The $\varkappa$-type salts such as $\varkappa$-$(BEDT\text{-}TTF)_2Cu(SCN)_2$ have large deviations in the electronic and magnetic properties[7] from the typical Mott insulators, as characterized with their weakly temperature-dependent small paramagnetic susceptibility and high electrical conductivity. Eventually, according to the present work, except for the salts along the metal–insulator boundary, the Mott insulator salts have common features; that is, the magnetic properties of the Mott insulators can be explained on the basis of the localized spin models regardless of the strength of the electron delocalization, as summarized in the next paragraph.

The β'-salts are characterized as a quasi-two-dimensional square lattice Heisenberg antiferromagnetic system with $J \approx -59$ K for both salts. Three-dimensional antiferromagnetic transitions take place at $T_N = 22$ and 28 K for the ICl_2 and $AuCl_2$ salts, respectively, in which the small

inter-layer interactions $J' \approx 1\times10^{-4}\,J$ and $1\times10^{-3}\,J$ play an important role. The magnetic structure of the $GaCl_4$ salt consists of two kinds of one-dimensional chain structures, where the presence of alternating inter-chain interactions adds a feature of a two-leg-ladder structure. The intra-chain interaction is estimated at $J \approx -70$ K, and the susceptibility decreasing to zero as the temperature approaches zero is consistent with the feature of the two-leg-ladder system. The α'-salt having weak dimerization shows the one-dimensional alternating chain structure of $J \approx -53$ and $J' \approx -26$ K, giving a spin-singlet ground state at $T = 0$ K. The crystal structure of the 3 : 1 ClO_4 salts forms weak trimerization with charge disproportionation giving one localized spin per trimer, resulting in a quasi-one-dimensional structure where the inter-chain interactions generate a frustration feature. The isostructural AsF_6 salt behaves similarly to the ClO_4 salt from the point of localized spin model in spite of the electron delocalization emerging at high temperatures.

The feature of the ESR line width in relation to the strength of dimerization/trimerization is considered to be responsible for the electron localization. For the β'-ICl_2, $GaCl_4$, and ClO_4 salts having strong electron localization, the ESR line widths can be explained in terms of the spin–spin relaxation similar to the ordinary localized spin systems, whereas the line widths of the α'-IBr_2 and AsF_6 salts are suggestive of the strong influence of the spin–lattice relaxation process associated with the electron delocalization. The most remarkable feature in the α'-IBr_2 and AsF_6 salts is reflected by the reduced magnetic moments, which are considered to feature the delocalization of the electrons on the weak dimer/trimer units. The above criteria on the electron localization/delocalization are reinforced by the fact that the $\varkappa$-type salts located around the metal–insulator boundary have a small magnetic moment[7] and a large ESR line width[43] of the spin–lattice relaxation origin.

This work is supported by a Grant-in-Aid for Scientific Research on Priority Areas (No.10149101 "Metal-assembled Complexes") from the Ministry of Education, Science, Sports and Culture. We thank Prof. T. Mori who provided samples of ET·$HgBr_3$, and Dr. J. Yamaura, Prof. K. Suzuki, and Prof. Y. Ajiro for helpful discussions.

References

1) M. Kobayashi, T. Enoki, K. Imaeda, H. Inokuchi, and G. Saito, *Phys. Rev. B*, **B36**, 1457 (1987).
2) S. D. Obertelli, R. H. Friend, D. R. Talham, M. Kurmoo, and P. Day, *J. Phys.: Condens. Matt.*, **1**, 5671 (1989).
3) N. Yoneyama, A. Miyazaki, and T. Enoki, unpublished.
4) J. Yamaura, A. Miyazaki, T. Enoki, and G. Saito, *Phys. Rev. B*, **B55**, 3649 (1997).
5) H. Ito, T. Ishiguro, M. Kubota, and G. Saito, *J. Phys. Soc. Jpn.*, **66**, 2987 (1996).
6) T. Naito, K. Bun, A. Miyamoto, H. Kobayashi, H. Sawa, R. Kato, and A. Kobayashi, *Synth. Met.*, **55-57**, 2234 (1993).
7) H. Urayama, H. Yamochi, G. Saito, K. Nozawa, T. Sugano, M. Kinoshita, S. Sato, K. Oshima, A. Kawamoto, and J. Tanaka, *Chem. Lett.*, **1988**, 55.
8) S. Klotz, J. S. Schilling, S. Gärtner, and D. Schweitzer, *Solid State Commun.*, **67**, 981 (1988).
9) D. R. Talham, M. Kurmoo, P. Day, D. S. Obertelli, I. D. Parker, and R. H. Friend, *J. Phys. C: Solid State Phys.*, **19**, L383 (1986).
10) M. Inoue and M. B. Inoue, *J. Chem. Soc., Chem. Commun.*, **1985**, 1043.
11) A. Miyazaki, I. Ichikawa, T. Enoki, and G. Saito, *Bull. Chem. Soc. Jpn.*, **70**, 2647 (1997).
12) K. Mortensen, Y. Tomkiewicz, and K. Bechgaard, *Phys. Rev. B*, **B25**, 3319 (1982).
13) P. J. Nigrey, B. Morosin, J. F. Kwak, E. L. Venturini, and R. J. Baughman, *Synth. Met.*, **16**, 1 (1986).
14) N. Yoneyama, A. Miyazaki, T. Enoki, and T. Mori, private communication.
15) T. Enoki, J. Yamaura, and A. Miyazaki, *Bull. Chem. Soc. Jpn.*, **70**, 2005 (1997).
16) H. Kobayashi, R. Kato, A. Kobayashi, G. Saito, M. Tokumoto, H. Anzai, and T. Ishiguro, *Chem. Lett.*, **1986**, 89.
17) T. J. Emge, H. H. Wang, P. C. W. Leung, P. R. Rust, J. D. Cook, P. L. Jackson, K. D. Carlson, J. M. Williams, M.-H. Whangbo, E. L. Venturini, J. E. Schirber, L. J. Azevedo, and J. R. Ferraro, *J. Am. Chem. Soc.*, **108**, 695 (1986).
18) T. Mori and H. Inokuchi, *Solid State Commun.*, **62**, 525 (1987).
19) T. J. Emge, H. H. Wang, M. K. Bowman, C. M. Pipan, K. D. Carlson, M. A. Beno, L. N. Hall, B. A. Anderson, J. M. Williams, and M.-H. Whangbo, *J. Am. Chem. Soc.*, **109**, 2016 (1987).
20) M. Kurmoo, M. Allan, R. H. Friend, D. Chasseau, G. Bravic, and P. Day, *Synth. Met.*, **41-43**, 2127 (1991).
21) M. Tokumoto, H. Anzai, T. Ishiguro, G. Saito, H. Kobayashi, R. Kato, and A. Kobayashi, *Synth. Met.*, **19**, 215 (1987).
22) M. Watanabe, M. Nishikawa, Y. Nogami, K. Oshima, and G. Saito, *J. Korean Phys. Soc.*, **31**, 95 (1997).
23) R. Kato, H. Kobayashi, A. Kobayashi, and Y. Sasaki, *Chem. Lett.*, **1984**, 1693.
24) R. Kato, H. Kobayashi, T. Mori, A. Kobayashi, and Y. Sasaki, *Solid State Commun.*, **55**, 387 (1985).
25) N. Yoneyama, A. Miyazaki, and T. Enoki, *Synth. Met.*, to be published.
26) J. M. Williams, H. H. Wang, M. A. Beno, T. J. Emge, L. M. Sowa, P. T. Copps, F. Behroozi, L. N. Hall, K. D. Carlson, and G. W. Crabtree, *Inorg. Chem.*, **23**, 3841 (1984).
27) T. Mori, A. Kobayashi, Y. Sasaki, H. Kobayashi, G. Saito, and H. Inokuchi, *Bull. Chem. Soc. Jpn.*, **57**, 627 (1984).
28) H. C. Montgomery, *J. Appl. Phys.*, **42**, 2971 (1971).
29) N. Yoneyama, A. Miyazaki, T. Enoki, and G. Saito, *Synth. Met.*, **86**, 2029 (1997).
30) N. Kinoshita, M. Tokumoto, H. Anzai, and G. Saito, *Synth. Met.*, **19**, 203 (1987).
31) M. E. Lines, *J. Phys. Chem. Solids*, **31**, 101 (1970).
32) F. Keffer, "Encyclopedia of Physics," ed by H. P. J. Wijn, Springer-Verlag, New York (1966), Vol. ÚXVIII/2, p. 124.
33) C. Coulon, R. Laversanne, J. Amiell, and P. Delhaes, *J. Phys. C: Solid State Phys.*, **19**, L753 (1986).
34) T. Oguchi, *Phys. Rev.*, **133**, A1098 (1964).
35) H. Seo and H. Fukuyama, *J. Phys. Soc. Jpn.*, **66**, 3352 (1997).
36) J. C. Bonner and M. E. Fisher, *Phys. Rev.*, **135**, A640 (1964).
37) W. Duffy and K. P. Barr, *Phys. Rev.*, **165**, 647 (1968).
38) T. Sugano, G. Saito, and M. Kinoshita, *Phys. Rev. B*, **B34**, 117 (1986).

39) N. Yoneyama, A. Miyazaki, and T. Enoki, private communications.
40) P. M. Chaikin and G. Beni, *Phys. Rev. B*, **B13**, 647 (1976).
41) Y. Ajiro, S. Matsukawa, T. Yamada, and T. Haseda, *J. Phys. Soc. Jpn.*, **39**, 259 (1975).
42) A. Miyazaki, T. Enoki, H. Uekusa, Y. Ohashi, and G. Saito, *Phys. Rev. B*, **B55**, 6847 (1997).
43) H. Urayama, H. Yamochi, G. Saito, S. Sato, T. Sugano, M. Kinoshita, A. Kawamoto, J. Tanaka, T. Inabe, T. Mori, Y. Maruyama, and H. Inokuchi, *Synth. Met.*, **27**, A393 (1988).